Journal of Advanced Research in Applied Sciences and Engineering Technology

Journal homepage:
https://semarakilmu.com.my/journals/index.php/applied_sciences_eng_tech/index
ISSN: 2462-1943

Impact on Reconstruction SPECT Image Distortion by Iteration and Subset Number

Mohd Akmal Masud[1,4], Mohd Zamani Ngali[2,*], Siti Amira Othman[1], Ishkrizat Taib[2], Kahar Osman[3], Salihatun Md Salleh[2], Ahmad Zahran Md. Khudzari[3], Nor Salita Ali[4], Anucha Chaichana[5]

[1] Faculty of Applied Sciences and Technology, Universiti Tun Hussein Onn Malaysia, 84600 Panchor, Johor, Malaysia
[2] Faculty of Manufacturing and Engineering, Universiti Tun Hussein Onn Malaysia, 86400 Batu Pahat Johor, Malaysia
[3] Faculty of Biosciences and Medical Engineering, Universiti Teknologi Malaysia, 81310 Johor Bahru, Johor, Malaysia
[4] Nuclear Medicine Department, National Cancer Institute, 62250 Putrajaya, Malaysia
[5] Faculty of Medical Technology, Department of Radiological Technology, Mahidol University, Bangkok 10700 Thailand

ARTICLE INFO

Article history:
Received 4 June 2023
Received in revised form 6 October 2023
Accepted 15 October 2023
Available online 31 October 2023

Keywords:
SPECT; Astonish; OSEM

ABSTRACT

Iterative reconstruction on Single Photon Emission Computed Tomography (SPECT) imaging has recently been commercially available, resulting in reconstructed images with lower noise levels and better spatial resolution. The reconstruction variables employed and chosen under these suggestions include post-filtering, as well as several iterations and subset numbers. However, most of the number of iterations and subsets will give distortion to the segmentation image on a volume to be segmented. For this purpose, this paper will compare the effect of distortion on the dice similarity coefficient of volume segmentation for the iterative reconstruction setting by default as practice. The best outcome with the smallest root-mean-square deviation, highest percentage contrast values, and highest dice similarity coefficient) for all iterations and subsets is in iteration 6 subset 16. Here, the root-mean-square deviation is 8.06. Moreover, the four most enormous spheres can be calculated from the six spheres filled. The best contrast percentage is in subset 32, but the background variability for that subset is exceptionally high, which is 64.5. With post-filtering implementation, the scatter-corrected slices show the most enhanced image resolution and contrast when using advanced Astonish reconstruction algorithms. The user must decide if noise reduction via post-filtering or increased image resolution is more suitable for a certain imaging process.

1. Introduction

Iterative reconstruction using Single Photon Emission Computed Tomography (SPECT) is frequently used in clinical practice and has significantly improved image quality recently. The majority of recent advancements included expanding the system model to include more variables to simulate the emission/detection process more precisely [1]. SPECT acquisitions are used to gather the photon

* *Corresponding author.*
E-mail address: zamani@uthm.edu.my

https://doi.org/10.37934/araset.33.2.5566

projection from source distribution to create three-dimensional (3D) images of gamma emitter distributions [2].

Following the acquisition of a SPECT study, trans-axial slices are computed utilizing mathematical techniques using emission scan projection data [3]. First, they proposed two-dimensional (2D) iterative reconstructions to substitute filtered back-projection (FBP) at about the same time. After implementing attenuation and scatter corrections, they moved on to 3D iterative processing in more recent years [4]. A satisfactory image quality that satisfies the clinical requirements for examinations is referred to as good imaging performance. However, keeping the dose at the lowest possible amount is acceptable [5]. Because of that, several reconstruction algorithm methods have been developed; there are two approaches to image reconstruction of SPECT imaging.

The first one is analytical reconstruction, and the second one is an iterative reconstruction [6]. The iterative reconstruction is classified into two categories: ordered subset expectation maximization (OSEM) as well as maximum-likelihood expectation maximization (MLEM). Currently, most of the SPECT modalities use iterative reconstruction [7]. In iterative reconstruction, subsets may naturally correspond to groups of projections. Meanwhile, subsets matching the processing of projections in opposing pairs are used in subsequent simulations, and additional options may be considered [8].

For the different modalities, the data were reconstructed via General Electric Evolution for Bone, Philips Astonish, or Siemens Flash3D of eight subsets, as well as different iterations [9]. Nevertheless, there is an exceptional procedure in Philip SPECT modalities called the Astonish reconstruction method. The Astonish reconstruction technique utilises a double filtering approach to mitigate noise and improve uniformity, which improves reconstruction accuracy [10].

Astonish refers to an OSEM iterative approach that lowers statistical noise, allowing for lower injected doses and faster acquisition time. Additionally, the Astonish algorithm offers signal-to-noise improvement, resulting in reasonable image quality with a shorter scan time while reducing motion-induced artefacts [11]. The Astonish software package uses the three-dimensional ordered subset expectation maximisation (3D-OSEM) algorithm for image reconstruction. The 3D-OSEM algorithm, based on the MLEM algorithm, models Poisson noise for counting statistics during data gathering and avoids the long-range noise texture (such as noise streaks) frequently present in FBP reconstructed images.

The use of 3D technology enables 3D resolution recovery to be incorporated during image reconstruction [12]. Hippeläinen *et al.*, evaluated the outcomes of several OSEM reconstruction techniques. They found that alignment performed at its best when the images were corrected for attenuation, scatter, detector response, and collimator response [13]. However, the standardization of protocols in each modality used does not take into account the distortion in a volume segmentation for each use of the number of iterations and subsets during image reconstruction.

Most studies only focus on evaluating the hot contrast sphere and background variability for SPECT images [14,15]. Nonetheless, a lack of studies has the effect of the number of iterations and subsets on image distortion during the reconstruction process [16,17]. Therefore, this study will focus on the effect of using iteration number and subset on distortion volume segmentation Astonish reconstruction method. In addition, this paper will present some novel Dice similarity measures of volume segmentation for various iterations and subsets.

The unique Graphic User Interface (GUI) known as Medical Image Analysis Version 2.5 (MIA) was used to assess the contrast noise ratio and background variability for every number iteration and subset as dependent variables in this study. Furthermore, the contrast sphere and background ratio will be evaluated to determine the best image quality for clinical practice. In addition, this study will

use the National Electrical Manufacturers Association (NEMA) phantom with six standard spheres with Iodine-131 (^{131}I) inside as a radiotracer for projection gamma emitter sources.

2. Methodology

2.1 Phantom Preparation

The comparison iteration and the subset of the advanced reconstruction algorithms Philips Astonish were performed with the NEMA 2007 NU-2 image quality phantom. The NEMA 2007-NU-2 standard's body phantom was utilized to evaluate the transaxially images' quality [18]. The NEMA 2007-NU-2 standard's image quality (IQ) phantom was used, although ^{131}I was used instead of 18F. The six spheres were filled with a ^{131}I solution that produced an 8:1 lesion-to-background ratio and had the following dimensions: 37 mm, 28 mm, 22 mm, 17 mm, 13 mm, and 10 mm. All six spheres were filled, having a concentration of 0.211 MBq/ml compared to the background phantom's concentration of 0.0253 MBq/ml.

On SPECT systems, the tomographic acquisitions were made by Philips BrightView-XCT with the JetStream as their workstation. All acquisitions followed the same protocol: 128 x 128 matrix size, 360 Single Photon Emission Computed Tomography (SPECT) with six steps, 40 frames per second, and a variable rotational radius according to the proximity to the phantom surface. An ordinary NECK SPECT SPECT Philips specification of 120 kV and 20 mAs scan was performed after the SPECT acquisition. The acquisition workstations scaled the CT data and utilized it to adjust for attenuation. According to measurements of a point source in water, Philips uses scatter kernels that have already been calculated [19].

The same image processing workstations usually used for SPECT reconstruction were used for the reconstructions: Philips Jet-Stream 3.0 (Software version: v. 4.0.3.5, 2009). Astonish reconstructions were performed with different iterations and subsets. Four iterations, namely 2, 4, 6, and 8, with subsets 8, 16, and 32, were used for comparison. A Hanning filter with a cut-off was set up for all modes of iterations and subsets.

2.2 Evaluation of Image Quality

The maximum count for the hot spheres is included in the trans axial slice of the NEMA image quality phantom, which was used to evaluate image quality. MATLAB R2022a was used as a medium to analyse the image quality. This GUI, called MIA 2.5, as shown in Figure 1, was developed by Laszlo Balkay (https://www.mathworks.com/matlabcentral/fileexchange/4706-mia-2-5?s_tid=srchtitle).

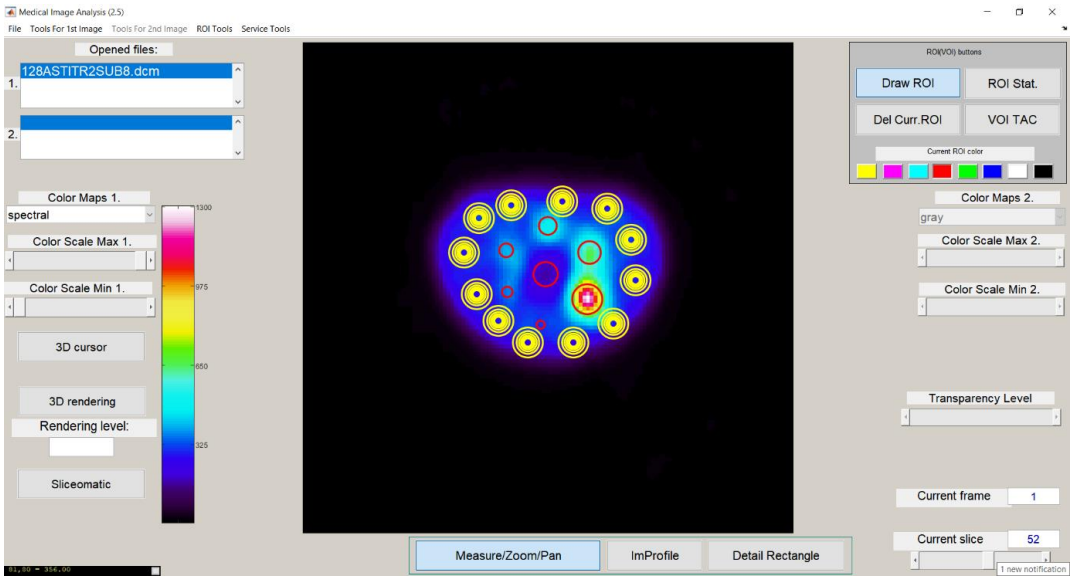

Fig. 1. Medical image analysis

The calculation of the contrast percentage for each hot sphere is as Eq. (1):

$$CS = \frac{C_{s,j}/C_b - 1}{R_s/R_b - 1} \times 100 \quad (1)$$

where $C_{s,j}$ identifies the counts in a circular region-of-interest (ROI) that is the same diameter as sphere j. The ratio of the activity concentration in the hot sphere to the activity concentration in the background is indicated by R_s/R_b. Meanwhile, C_b stands for the average counts of background ROIs of equal size. The percentage of background variability, BV, is as in Eq. (2):

$$BV = \frac{SD_b}{C_b} \times 100 \quad (2)$$

where, SD_b is the standard deviation for background ROI.

Image distortion is evaluated from the IQ images, while aspect ratio is defined as the ratio of the volume calculation divided by the actual volume. The best-fitting ellipse to a contour and isosurface function was derived utilizing MATLAB R2022a [20] to capture the best volume calculation distortion. Figures 2(a), 3(a), and 4(a) demonstrate results from the volume calculation distortion.

2.3 Distortion Evaluation

The Dice Similarity Coefficient is a measure of correspondence between two sets [21], as well as being used in the context of image segmentation to be defined as two times the volume of the overlap between two volumes of interest (VOI) divided by the total sum of the VOIs volumes. The original volume segmentation is done by setting the percentage of the maximum count on each sphere until the actual volume is obtained. Other than that, the reference image used is the image on iteration 2 and subset 8. This is because this image has a reconstruction image similar to the actual volume [22,23] For segmentation, after iteration and subsets are used, volume segmentation is performed on the sphere given as in Eq. (3).

$$DSC = \frac{2.|X \cap Y|}{|X| + |Y|} \quad (3)$$

where X is the original volume segmentation and Y is the segmentation volume sphere after an iteration and subset number reconstruction.

3. Results and Discussion

3.1 Image Contrast and Background Variability

The total effect of advanced reconstruction is portrayed in Table 1, where it is the background variability for iterations 2, 4, 6, 8, and subsets 8, 16, and 32. Meanwhile, the slices of the contrast image quality phantom that have been reconstructed are displayed in Figures 2, 3, and 4.

Table 1
Background variability for different iterations and subsets

Iteration	Subset	Background Variability
2	8	27.72
4	8	32.95
6	8	39.11
8	8	43.03
2	16	32.52
4	16	43.86
6	16	50.18
8	16	54.05
2	32	45.11
4	32	54.99
6	32	59.91
8	32	64.5

All iterations and subsets for Astonish's advanced reconstruction modes resulted in increased background variability when the number of iterations and subsets was raised, as shown in Figure 2.

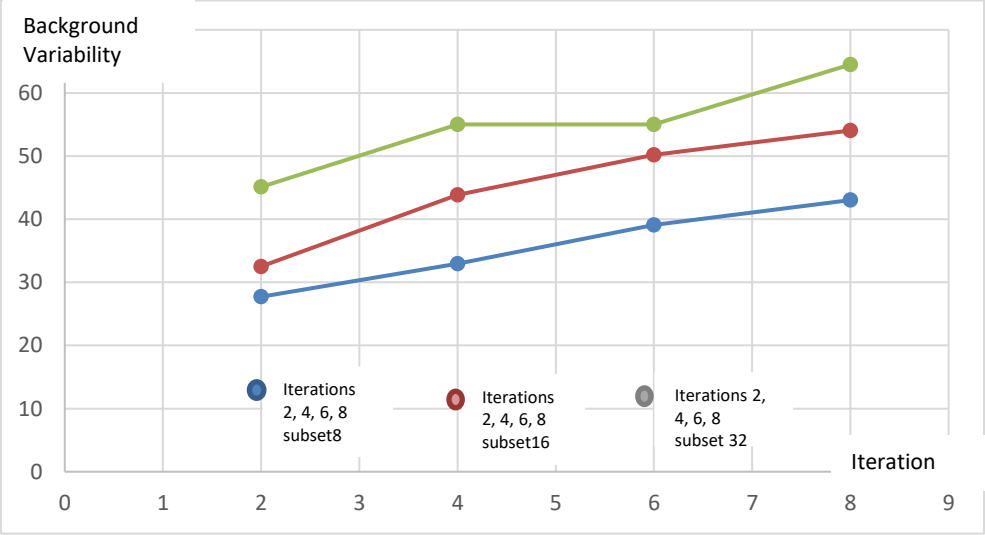

Fig. 2. Iteration affected on background variability

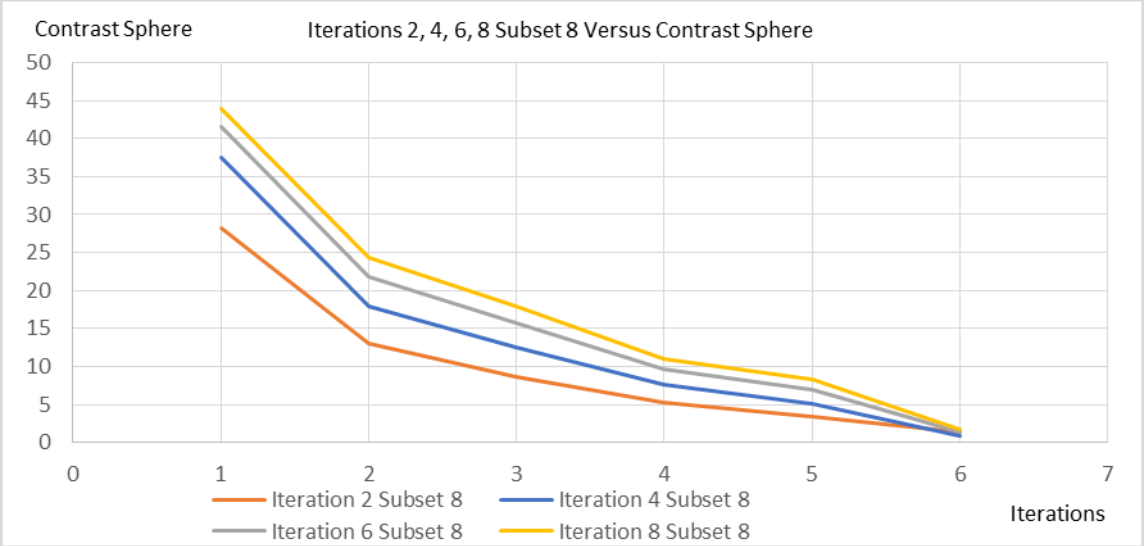

Fig. 3. Iterations 2, 4, 6, 8; subset 8 versus contrast sphere

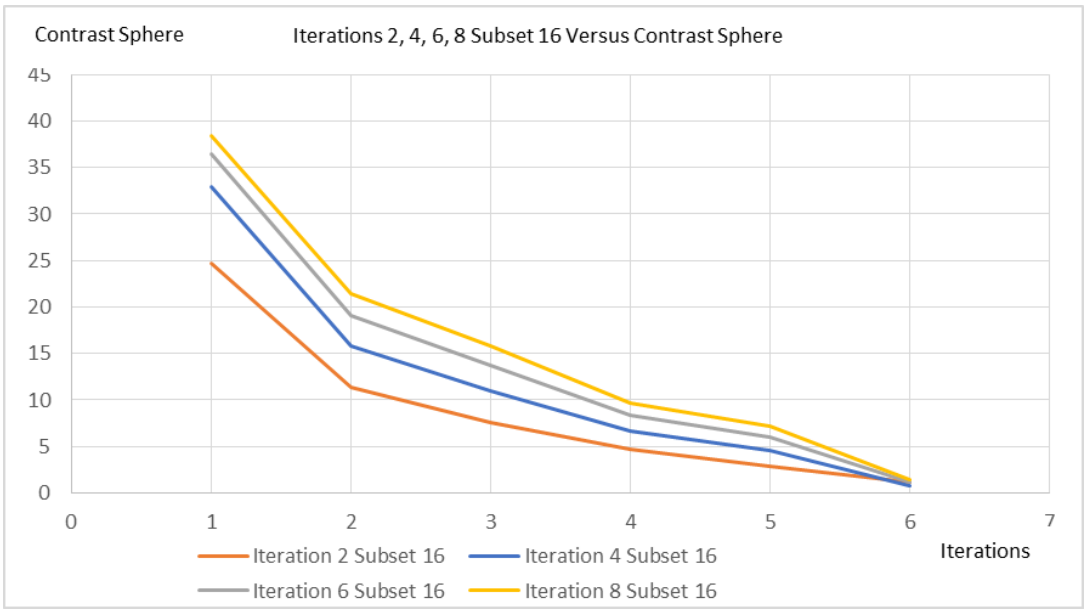

Fig. 4. Iterations 2, 4, 6, 8; subset 16 versus contrast sphere

For iterations 2, 4, 6, 8, and subset 8 as in Figure 5; the background variability is 27.72, 32.95, 39.11, and 43.03, respectively. For iterations 2, 4, 6, 8, and subset 16 as in Figure 6; the background variability is 32.52, 43.86, 50.18 and 54.05, respectively. For iterations 2, 4, 6, 8, and subset 32 as in Figure 7; the background variability is 45.11, 54.99, 59.91, and 64.50, respectively.

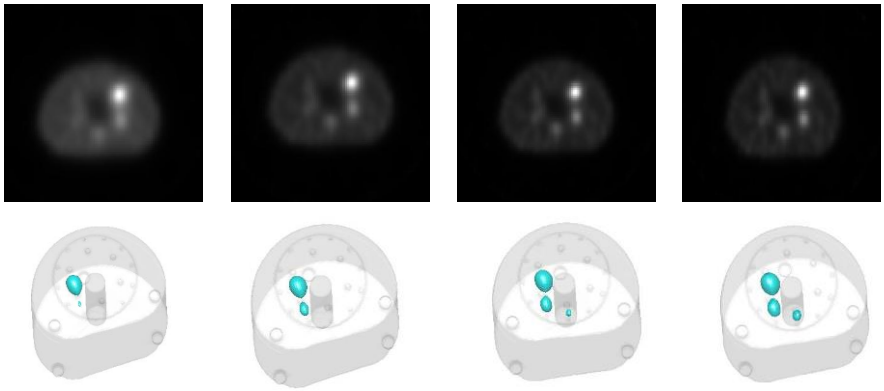

Fig. 5. Iterations 2, 4, 6, 8, and subsets 8

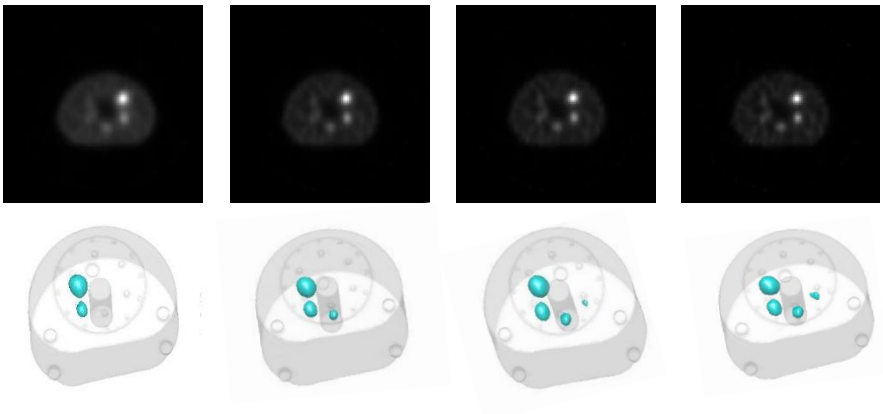

Fig. 6. Iterations 2, 4, 6, 8, and subsets 16

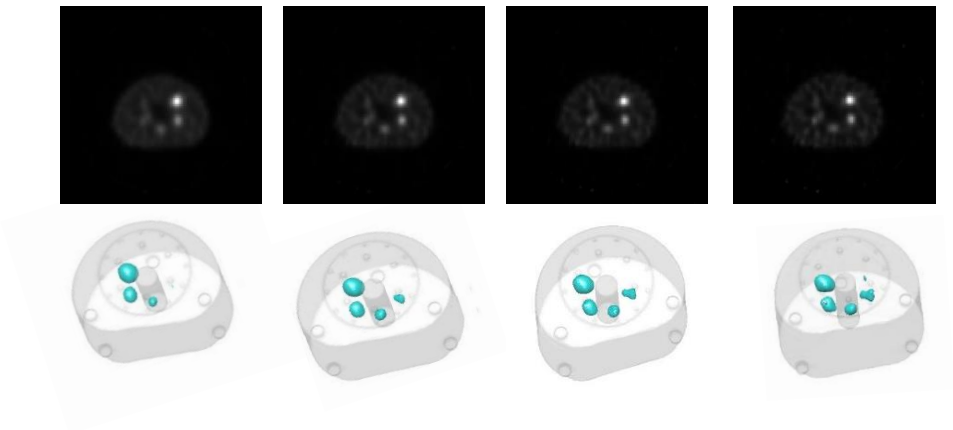

Fig. 7. Iterations 2, 4, 6, 8, and subsets 32

The contrasting percentage shows that the contrast percentage increased from spheres 1 to 6 for all iterations and subsets, as shown in Tables 2, 3, and 4. This demonstrates that when the number of iterations, as well as subsets, were raised, the contrast percentage decreased. For all iterations and subset numbers for Sphere 1, Sphere 2, and Sphere 3, the contrast percentage is lower than 20%. However, Sphere 6 has the highest contrast percentage for all iterations and subset numbers. As for the graph iteration, iterations 2, 4, 6, and 8 with subset 32, as shown in Figure 7, indicate the existence of significant non-uniformity of the contrast percentage.

Table 2
Contrast Noise Ratio for Iterations 2, 4, 6, 8; Subset 8

Iteration 2 Subset 8		Iteration 4 Subset 8		Iteration 6 Subset 8		Iteration 8 Subset 8	
Sphere	CNR	Sphere	CNR	Sphere	CNR	Sphere	CNR
1	28.25	1	37.56	1	41.63	1	43.89
2	12.97	2	18.00	2	21.75	2	24.42
3	8.61	3	12.51	3	15.68	3	17.97
4	5.32	4	7.64	4	9.59	4	11.07
5	3.33	5	5.17	5	6.90	5	8.25
6	1.32	6	0.91	6	1.33	6	1.69

Table 3
Contrast Noise Ratio for Iterations 2, 4, 6, 8; Subset 16

Iteration 2 Subset 16		Iteration 4 Subset 16		Iteration 6 Subset 16		Iteration 8 Subset 16	
Sphere	CNR	Sphere	CNR	Sphere	CNR	Sphere	CNR
1	24.76	1	32.92	1	36.49	1	38.47
2	11.37	2	15.77	2	19.06	2	21.40
3	7.55	3	10.97	3	13.74	3	15.75
4	4.66	4	6.70	4	8.40	4	9.70
5	2.92	5	4.54	5	6.05	5	7.23
6	1.16	6	0.80	6	1.17	6	1.48

Table 4
Contrast Noise Ratio for Iterations 2, 4, 6, 8; Subset 32

Iteration 2 Subset 32		Iteration 4 Subset 32		Iteration 6 Subset 32		Iteration 8 Subset 32	
Sphere	CNR	Sphere	CNR	Sphere	CNR	Sphere	CNR
1	48.37216	1	45.9583	1	48.28086	1	48.39543
2	36.19233	2	23.55971	2	32.48984	2	34.77807
3	22.92848	3	16.84782	3	21.10825	3	22.34467
4	19.62427	4	12.93473	4	15.35933	4	17.69682
5	13.39993	5	7.573357	5	11.04244	5	12.56456
6	2.910616	6	0.610675	6	2.33346	6	2.582524

The image distortion was evaluated using images from the image quality (IQ) phantom. Figure 8 summarises the root-mean-square deviation (RMSD), which visually represents the scenario of a rebuilt sphere distorted into the shape of an ellipse. Generally, increasing the number of iterations and subsets of Astonish advanced reconstruction modes increases the image's ability to separate between the lesion and the background.

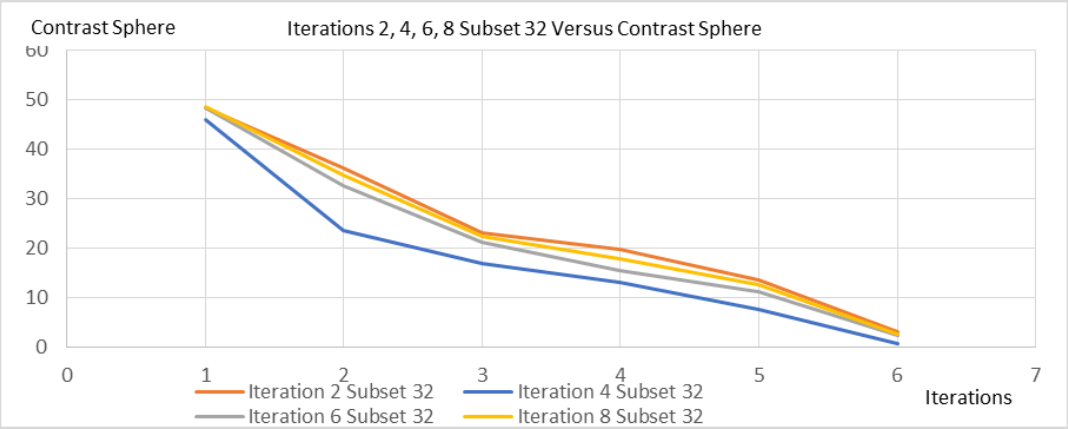

Fig. 8. Iterations 2, 4, 6, 8; subset 32 versus contrast sphere

The result shows that iteration 8 subset 32 had the highest number of lesions. Five lesions can be calculated from the six spheres. Furthermore, iteration 2 subset 8 was the lower number of lesions that can be shown. Two lesions can be calculated from the six spheres, supposedly. Nevertheless, all the iterations and subsets cannot be calculated for all six spheres. Although iteration 8 subset 32 can calculate the five spheres, the percentage distortion is very high compared to iteration 2 subset 8.

3.2 Distortion

The image distortion was evaluated using images from the IQ phantom. Table 5 summarises the RMSD for volume calculation of the Dice Similarity Coefficient, which visually represents the scenario of a reconstructed sphere that has been distorted into a sphere. Generally, increasing the number of iterations and subsets of Astonish advanced reconstruction modes increases the image's ability to separate between the lesion and the background.

Table 5
Image distortion for iterations 2, 4, 6, 8; subsets 8, 16, 32

Iteration	Subset	Sphere 1 (ml)	Sphere 2 (ml)	Sphere 3 (ml)	Sphere 4 (ml)	Sphere 5 (ml)	Sphere 6 (ml)	Root-Mean-Square Deviation	Dice Similarity Coefficient
2	8	21.08	1.73	-	-	-	-	283.28	0.32
4	8	22.48	5.45	-	-	-	-	56.23	0.41
6	8	23.78	8.46	2.37	-	-	-	46.64	0.46
8	8	26.37	10.68	4.64	-	-	-	7.18	0.52
2	16	24.42	7.22	0.00	-	-	-	29.83	0.66
4	16	26.26	10.57	4.21	-	-	-	11.21	0.71
6	16	26.26	12.24	6.42	1.99	-	-	8.08	0.86
8	16	26.10	12.56	7.12	3.46	-	-	8.68	0.61
2	32	26.74	10.46	4.58	1.29	-	-	25.36	0.54
4	32	25.88	11.97	7.01	4.53	-	-	12.03	0.51
6	32	25.61	11.70	7.33	6.31	-	-	16.02	0.42
8	32	26.42	11.92	7.98	7.44	2.43	-	17.86	0.45

It can be noted here that, for the dice similarity coefficient, iteration 6 with subset 16 has the highest dice, which is 0.86 compared to the other 11 settings. On the other hand, although iteration 8 with subset 32 can distinguish five spheres from the background, the dice similarity is very low, which is only 0.45.

In nuclear medicine, iterative reconstruction approaches for reconstructing Single Photon Emission Computed Tomography (SPECT) data are currently the most commonly used. However, by strengthening the mathematical modelling of the acquisition procedure, it is possible to significantly enhance the transaxial slices' image quality. Therefore, three subsets and four iterations of Philips' Astonish advanced iterative algorithms that use the function of the detector response during the reconstruction process via image quality measurement were compared in this study. Meanwhile, four iterations of 2, 4, 6, and 8 were used for the reconstruction process criteria (e.g., number of iterations and subsets). Moreover, subsets 8, 16, and 32 were used in this research. In this work, all the various parameters reconstruction methods Philips Astonish were tested to be clinically reasonable.

With the help of the NEMA image quality phantom, their performance was examined. Phantoms were obtained using cutting-edge SPECT systems: Philips BrightView XCT. The phantoms were acquired properly according to the standard clinical guidelines for bone research. Subsequently, the data were used to reconstruct advanced reconstruction algorithms with various settings. This design

was chosen to assess the algorithms' performance utilising the manufacturers' recommendations, which are the reconstruction parameters that are most frequently employed in clinical practice.

The number of iterations and subsets employed by the different methods and the recommended post-filters range greatly between the systems that implement the post-filtering using the conventional method (Philips: Hanning). The result obtained in this work shows that iteration 2 with subset 8 has lower background variability compared to other iterations and subsets. Meanwhile, iteration 8 with subset 32 shows the highest background variability. According to Zimmerman [24], an image with lower background variability is more significant to implement in clinical practice practically. If the background has low variability, it is the most accessible to differentiate the lesion background.

On the other hand, the contrast percentage evaluation increases from Sphere 1 to Sphere 6. For the biggest sphere (Sphere 1), there is a difference in contrast between the sphere and the background. This is because Sphere 1 has a high mean count compared to Sphere 2 and Sphere 3. For Spheres 4, 5, and 6, the contrast percentage is under 20% because the mean counts are almost identical to the mean counts in the background. This is also due to the small volume's poor spatial resolution in SPECT imaging with a diameter below 20 mm.

However, looking at iterations 2, 4, 6, and 8 with subset 32, the percentage contrast supposedly becomes lower than that of iterations 2, 4, 6, and 8 with subset 16 due to the high ability of the Astonish algorithm to localise the sphere between the backgrounds. However, the distortion and the background variability itself must be considered. Although iterations 2, 4, 6, and 8 with subset 32 have high contrast, the background variability and geomean percentage distortion are also very high. In addition, the low accuracy of the calculation volume makes it difficult for the physician to differentiate the lesions and background if qualitative visualisation is used.

Observing the distortion aspect, the best setting is iteration 6 and subset 16. This setting will calculate the four lesions with a geomean of only 8.06%. Even though iteration 8 with subset 32 can calculate five lesions, the distortion percentage is very high. Therefore, the vendors recommended using only iteration 2 with subset 8 for the Astonish reconstruction method. Increasing the number of iterations and subsets, the time will increase to reconstruct the image, thus rendering it an impractical routine practice.

4. Conclusions

This study has found that the iterations and subsets numbers on the Astonish reconstruction method have a big effect on quality images. In this paper, a best iteration and subset number for high accuracy dice similarity coefficient is proposed. The main contribution of this work is to evaluate the image quality using medical image Analysis (MIA 2.5) and to determine the high accuracy for volume segmentation on targeted volume. Although the Astonish algorithm leads to a visual with a contrasting image and lowering noise, the overshoot artefact can be one type of reconstruction's drawbacks. Before using images that have been restored using this algorithm, it is advised that quantitative applications be given great thought. The amount of this artefact could be decreased by sampling projection data more frequently. This has been made possible by the noise reduction provided by the Hanning filter throughout the rebuilding process. Apart from that, the findings of this work thus support the idea that collimators with all purposes can be utilised for Astonish Single Photon Emission Computed Tomography (SPECT) imaging instead of collimators with high resolution.

Acknowledgement
The authors would like to thank the Director General of Health Malaysia for the permission to publish this paper and want to express gratitude to Institut Kanser Negara for the facilities provided. The funding for the project has been provided by Kementerian Pengajian Tinggi Malaysia (KPTM) under the FRGS grant (Grant No: FRGS/1/2019 Vot K200) that made the research possible. Ethical approval for this study was obtained from the Medical Research and Ethics Committee (MREC), Ministry of Health Malaysia (NMRR-20-1239-53306).

References

[1] Lima, Thiago VM, Ujwal Bhure, Maria de Sol Pérez Lago, Yannick Thali, Savo Matijasevic, Justus Roos, and Klaus Strobel. "Impact of metal implants on xSPECT/CT Bone reconstruction: the “shining metal artefact”." *European journal of hybrid imaging* 4, no. 1 (2020): 1-6. https://doi.org/10.1186/s41824-020-00087-7

[2] Franc, Benjamin L., Paul D. Acton, Carina Mari, and Bruce H. Hasegawa. "Small-animal SPECT and SPECT/CT: important tools for preclinical investigation." *Journal of nuclear medicine* 49, no. 10 (2008): 1651-1663. https://doi.org/10.2967/jnumed.108.055442

[3] Knoll, Peter, Daniela Kotalova, Gunnar Köchle, Ivan Kuzelka, Greg Minear, Siroos Mirzaei, Martin Šámal, Ladislav Zadrazil, and Helmar Bergmann. "Comparison of advanced iterative reconstruction methods for SPECT/CT." *Zeitschrift für medizinische Physik* 22, no. 1 (2012): 58-69. https://doi.org/10.1016/j.zemedi.2011.04.007

[4] Seret, Alain, Daniel Nguyen, and Claire Bernard. "Quantitative capabilities of four state-of-the-art SPECT-CT cameras." *EJNMMI research* 2, no. 1 (2012): 1-19. https://doi.org/10.1186/2191-219X-2-45

[5] Mansour, Z., A. Mokhtar, A. Sarhan, M. T. Ahmed, and T. El-Diasty. "Quality control of CT image using American College of Radiology (ACR) phantom." *The Egyptian journal of Radiology and nuclear medicine* 47, no. 4 (2016): 1665-1671. https://doi.org/10.1016/j.ejrnm.2016.08.016

[6] Hsieh, Jiang, Brian Nett, Zhou Yu, Ken Sauer, Jean-Baptiste Thibault, and Charles A. Bouman. "Recent advances in CT image reconstruction." *Current Radiology Reports* 1 (2013): 39-51. https://doi.org/10.1007/s40134-012-0003-7

[7] Wang, Dong, Haohan Li, Xiaoyu Wei, and Xiao-Ping Wang. "An efficient iterative thresholding method for image segmentation." *Journal of Computational Physics* 350 (2017): 657-667. https://doi.org/10.1016/j.jcp.2017.08.020

[8] Lyra, Maria, Agapi Ploussi, Maritina Rouchota, and Stella Synefia. "Filters in 2D and 3D cardiac SPECT image processing." *Cardiology research and practice* 2014 (2014). https://doi.org/10.1155/2014/963264

[9] Onishi, Hideo, Nobutoku Motomura, Koichi Fujino, Takahiro Natsume, and Yasuhiro Haramoto. "Quantitative performance of advanced resolution recovery strategies on SPECT images: evaluation with use of digital phantom models." *Radiological physics and technology* 6 (2013): 42-53. https://doi.org/10.1007/s12194-012-0168-z

[10] O’Mahoney, Eoin, and Iain Murray. "Evaluation of a matched filter resolution recovery reconstruction algorithm for SPECT-CT imaging." *Nuclear medicine communications* 34, no. 3 (2013): 240-248. https://doi.org/10.1097/MNM.0b013e32835ce5b5

[11] Zohaib, Ali, Muhammad Hamid Saeed, Shaukat Ali Shahid, Muhammad Shahbaz, Mudassar Iqbal, and Faisal Ehsan. "Myocardial Perfusion Imaging (MPI): Superior Clinical Performance, A Comparison Between Filtered Backprojection (FBP) And Astonish Iterative Reconstruction Method With Cardiac Catheterization." *The Professional Medical Journal* 23, no. 04 (2016): 451-459. https://doi.org/10.29309/TPMJ/2016.23.04.1504

[12] Maeda, Yukito, Akio Nagaki, Yoshihiro Komi, Nobukazu Abe, and Shinya Kashimura. "Evaluation of resolution correction in single photon emission computed tomography reconstruction method using a body phantom: Study of three different models." *Nihon Hoshasen Gijutsu Gakkai Zasshi* 71, no. 11 (2015): 1070-1079. https://doi.org/10.6009/jjrt.2015_JSRT_71.11.1070

[13] Ramonaheng, Keamogetswe, Johannes A. van Staden, and Hanlie du Raan. "The effect of calibration factors and recovery coefficients on 177Lu SPECT activity quantification accuracy: a Monte Carlo study." *EJNMMI physics* 8, no. 1 (2021): 1-23. https://doi.org/10.1186/s40658-021-00365-8

[14] Demir, Mustafa, Mohammad Abuqbeitah, Nami Yeyin, and Kerim Sönmezoğlu. "Comparison between PET/MR and PET/CT: NEMA tests and image quality." *Turkish Journal of Oncology* 32, no. 3 (2017). https://doi.org/10.5505/tjo.2017.1599

[15] Kaiser, L. G. M., S. A. Ahmadi, M. Unterrainer, A. Holzgreve, E. Mille, A. Gosewisch, J. Brosch *et al.,* "Annual Congress of the European Association of Nuclear Medicine October 12–16, 2019 Barcelona, Spain." *Eur J Nucl Med Mol Imaging* 46 (2019): 1-952. https://doi.org/10.1007/s00259-019-04486-2

[16] Perez, Kristy L., Spencer J. Cutler, Priti Madhav, and Martin P. Tornai. "Towards quantification of functional breast images using dedicated SPECT with non-traditional acquisition trajectories." *IEEE transactions on nuclear science* 58, no. 5 (2011): 2219-2225. https://doi.org/10.1109/TNS.2011.2165223

[17] Mahmood, Usman, David DB Bates, Yusuf E. Erdi, Lorenzo Mannelli, Giuseppe Corrias, and Christopher Kanan. "Deep learning and domain-specific knowledge to segment the liver from synthetic dual energy ct iodine scans." *Diagnostics* 12, no. 3 (2022): 672. https://doi.org/10.3390/diagnostics12030672

[18] Yoon, Hyun Jin, Young Jin Jeong, Hye Joo Son, Do-Young Kang, Kyung-Yae Hyun, and Min-Kyung Lee. "Optimization of the spatial resolution for the GE discovery PET/CT 710 by using NEMA NU 2-2007 standards." *Journal of the Korean Physical Society* 66 (2015): 287-294.

[19] Heller, G. V., T. M. Bateman, S. J. Cullom, H. H. Hines, and A. J. Da Silva. "Improved clinical performance of myocardial perfusion SPECT imaging using Astonish iterative reconstruction." *Philips MedicaMundi* 53, no. 3 (2009): 43-9.

[20] Taha, Abdel Aziz, and Allan Hanbury. "Metrics for evaluating 3D medical image segmentation: analysis, selection, and tool." *BMC medical imaging* 15, no. 1 (2015): 1-28. https://doi.org/10.1186/s12880-015-0068-x

[21] Gustafsson, Johan, Anna Sundlöv, and Katarina Sjögreen Gleisner. "SPECT image segmentation for estimation of tumour volume and activity concentration in 177 Lu-DOTATATE radionuclide therapy." *EJNMMI research* 7 (2017): 1-17. https://doi.org/10.1186/s13550-017-0262-7

[22] Deye, Nicolas, François Vincent, Philippe Michel, Stephan Ehrmann, Daniel Da Silva, Michael Piagnerelli, Antoine Kimmoun *et al.,* "Changes in cardiac arrest patients' temperature management after the 2013 "TTM" trial: results from an international survey." *Annals of intensive care* 6, no. 1 (2016): 1-9. https://doi.org/10.1186/s13613-015-0104-6

[23] Husin, Akmal Hakim, Syahmil Hakim Hamzani, Shahrin Hisham Amirnordin, Mohd Faizal Mohideen Batcha, Rafiuddin Wahidon, and Makatar Wae-hayee. "Drying Studies of Oil Palm Decanter Cake for Production of Green Fertilizer." *Journal of Advanced Research in Fluid Mechanics and Thermal Sciences* 97, no. 2 (2022): 66-79. https://doi.org/10.37934/arfmts.97.2.6679

[24] Zimmerman, Brian E., Darko Grošev, Irène Buvat, Marco A. Coca Pérez, Eric C. Frey, Alan Green, Anchali Krisanachinda *et al.,* "Multizentrische Evaluierung der Genauigkeit und Präzision bei der Quantifizierung planarer Bildgebung und SPECT: Eine Phantomstudie der IAEA." *Zeitschrift fur Medizinische Physik* 27, no. 2 (2017): 98-112. https://doi.org/10.1016/j.zemedi.2016.03.008